6

Particle Formation in Combustion

Combustion processes emit large quantities of particles to the atmosphere. Particles formed in combustion systems fall roughly into two categories. The first category, referred to as ash, comprises particles derived from noncombustible constituents (primarily mineral inclusions) in the fuel and from atoms other than carbon and hydrogen (so-called heteroatoms) in the organic structure of the fuel. The second category consists of carbonaceous particles that are formed by pyrolysis of the fuel molecules.

Particles produced by combustion sources are generally complex chemical mixtures that often are not easily characterized in terms of composition. The particle sizes vary widely, and the composition may be a strong function of particle size. This chapter has a twofold objective—to present some typical data on the size and chemical composition of particulate emissions from combustion processes and to discuss the fundamental mechanisms by which the particles are formed.

6.1 ASH

Ash is derived from noncombustible material introduced in the combustor along with the fuel and from inorganic constituents in the fuel itself. The ash produced in coal combustion, for example, arises from mineral inclusions in the coal as well as from heteroatoms, which are present in the coal molecules. Heavy fuel oils produce much less ash than coals since noncombustible material such as mineral inclusions is virtually absent in such oils and heteroatoms are the only source of ash. Fuel additives ranging from lead used to control "knock" in gasoline engines, to barium for soot control in

diesel engines, to sulfur capture agents also contribute to ash emissions. We focus our discussion of ash on the particles produced in coal combustion.

6.1.1 Ash Formation from Coal

Ash particles produced in coal combustion have long been controlled by cleaning the flue gases with electrostatic precipitators (see Chapter 7). Most of the mass of particulate matter is removed by such devices, so ash received relatively little attention as an air pollutant until Davison et al. (1974) showed that the concentrations of many toxic species in the ash particles increased with decreasing particle size, as illustrated in Figure 6.1. Particle removal techniques, as we shall see in Chapter 7, are less effective for small (i.e., submicron) particles than for larger particles. Thus, even though the total

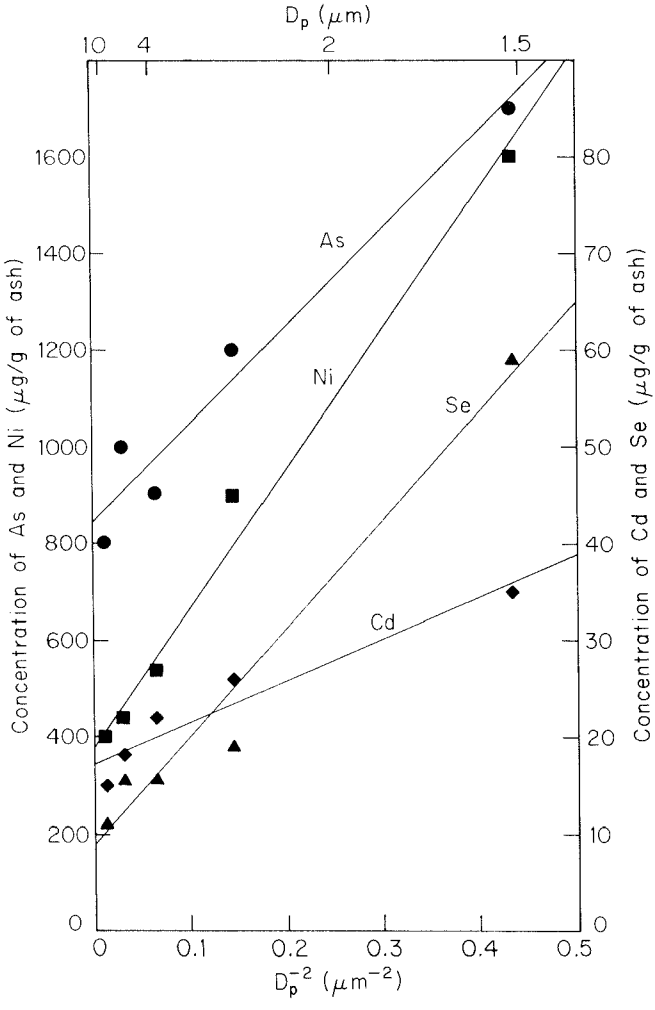

Figure 6.1 Variation of trace element concentrations with particle size for fly ash particles produced by coal combustion (data from Davison et al., 1974). The lower axis reflects the size dependence of the condensation rate.

mass of particulate matter in the flue gases may be reduced substantially by electrostatic precipitation or another system, the particles that do escape collection are those that contain disproportionately high concentrations of toxic substances.

Coal is a complex, heterogeneous, and variable substance containing, in addition to the fossilized carbonaceous material, dispersed mineral inclusions. The sizes of these inclusions vary from one coal to another and also depend on the way the coal is prepared. The mean diameter of the mineral inclusions is typically about 1 μm. These inclusions, consisting of aluminosilicates with pyrites, calcites, and magnesites in various proportions, eventually form ash particles as the carbon burns out. The ash particles that are entrained in the combustion gases are called *fly ash*.

In the coal combustion process in most power plants, crushed coal from the mine is pulverized into a fine powder (typically, 40 to 80 μm mass median diameter) and blown into the furnace with carrier air. The coal particles are heated by radiation and conduction from hot gases up to temperatures in excess of 1500 K. As a coal particle is being heated, it may mechanically break up into fragments because of thermal stresses induced by internal fissures, cracks, and structural imperfections initially present. Volatile fractions originally present in the coal or formed by pyrolysis are vaporized, and the particle may burst open from the internal evolution of such gases. Also, a heated coal particle may swell and become more porous. As the particle burns, pores in the carbon matrix open and the porosity increases further. Ultimately, the particle becomes so porous that it disintegrates into a number of fragments, each of which may contain a fraction of the mineral matter that was present in the parent coal particle.

Studies of the evolution of ash during pulverized coal combustion have revealed two major mechanisms by which ash particles formed (Flagan and Friedlander, 1978). First, ash residue particles that remain when the carbon burns out account for most of the mineral matter in the raw coal. The sizes of these particles are determined by the combustion process as follows: As the carbon is consumed, mineral inclusions come into contact with one another, forming larger ash agglomerates. Since the temperature of a burning pulverized coal particle is generally high enough that the ash melts, these agglomerates coalesce to form large droplets of molten ash on the surface of the burning char. The fragmentation of the char limits the degree of agglomeration of the ash within a single fuel particle, so a number of ash residue particles are produced from each parent coal particle. The largest of these ash particles typically contains a significant fraction (5 to 30%) of the ash in the initial fuel particle, but many smaller ash particles are also generated. The smallest of the ash residue particles are comparable in size to the mineral inclusions in the unburned fuel. The minimum size of the ash fragments formed in this manner is determined by the size distribution of the inclusions within the coal, typically ranging from a few tenths of a micrometer to several micrometers.

The residual ash particles include some intriguing structures. The ash melts at the high temperatures encountered in pulverized coal combustion and, due to the action of surface tension, coalesces into spherical particles. Gas evolution within the molten ash leads to the formation of hollow particles, known as *cenospheres*, some of which contain large numbers of smaller particles. Figure 6.2 shows such particles produced in the

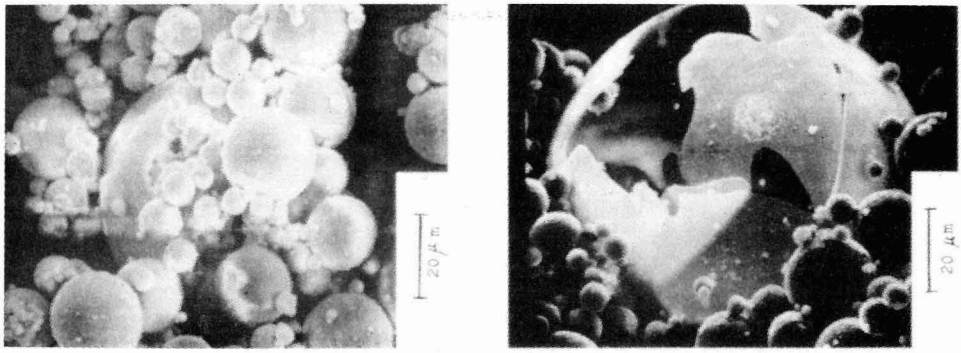

(a) (b)

Figure 6.2 Scanning electron microscope photographs of ash particles produced in the complete combustion of a lignite coal. Photograph (a) shows a large ash cenosphere containing many smaller spheres. Photograph (b) shows a large broken cenosphere on which the thin cenosphere wall can be seen (courtesy of A. F. Sarofim).

combustion of a lignite coal. These large, picturesque particles receive disproportionate attention, since dense particles generally account for most of the mass.

The second ash particle formation mechanism involves that small fraction of the ash, on the order of 1%, that vaporizes due to the high combustion temperatures. Part of the volatilized ash homogeneously nucleates to form very small (on the order of a few angstroms in size) particles, which then grow by coagulation and condensation of additional vaporized ash. At high temperatures, the agglomerated particles may coalesce into dense spheres, but after the combustion gases cool below the melting point of the condensed material, the liquid freezes and coalescence effectively ceases. Coagulation of the resulting solid particles produces chain agglomerates such as those shown in Figure 6.3. The chain agglomerate structure is a common feature of aerosols produced by vapor nucleation in high-temperature systems. It is also observed in carbonaceous soot aerosols and in the particles produced by a variety of high-temperature combustion processes.

Particle growth by coagulation leads to a predicted narrow mode in the particle size distribution in the size range 0.01 to 0.1 μm, much smaller than the mineral inclusions present in most coals. The remaining portion of the volatilized ash heterogeneously condenses on existing particles, including those formed by homogeneous nucleation and residual ash fragments. The ash formation process is depicted in Figure 6.4.

Measured particulate size distributions in the flue gases of pulverized coal combustion systems tend to support these two mechanisms for ash particle formation. Most of the mass of ash is generally above 1 μm in size, with a broad peak in the range 3 to 50 μm diameter. This large-diameter mode can be explained by the ash residue model. Submicron ash usually comprises less than 2% of the total fly ash mass. Figure 6.5 shows the size distributions measured immediately upstream of the electrostatic precipitator on a coal-fired utility boiler. The two distinct modes are readily apparent.

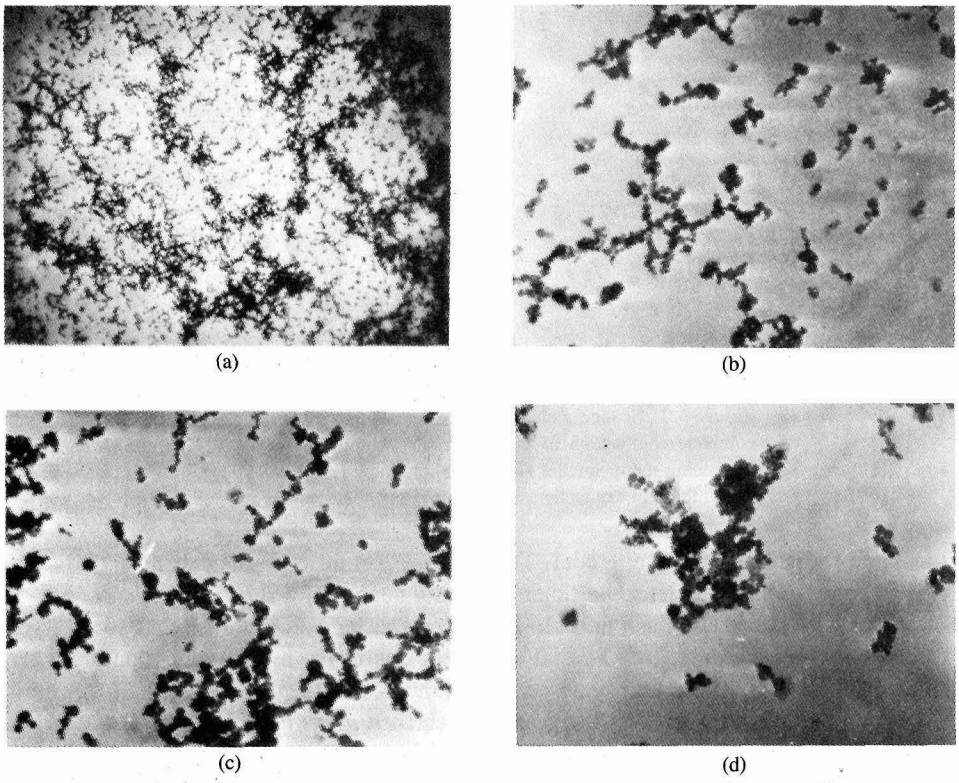

Figure 6.3 Transmission electron microscope photographs of the submicron ash fume produced in the combustion of entrained coal particles. The average sphere size is 20 to 30 nm (courtesy of A. F. Sarofim).

6.1.2 Residual Ash Size Distribution

In laboratory studies of the combustion of entrained coal particles, Sarofim et al. (1977) observed that the largest ash particles are significantly larger than the mineral inclusions in the coal from which the ash was derived, suggesting that the mineral inclusions coalesce on the surface of the burning char. Evidence for char fragmentation was also reported. Flagan and Friedlander (1978) used these observations in a first attempt to predict the size distribution of the ash residue particles, assuming that a number of equal-sized ash particles were produced from each parent coal particle and that the ash was uniformly distributed in the coal.

Neither of these assumptions is strictly true. Pulverizers used on coal-fired boilers generally employ aerodynamic classification to ensure that only particles that have been ground to a size sufficiently small to be burned completely within the combustor are sent to the burner. Because the aerodynamic diameter depends on density, mineral-rich par-

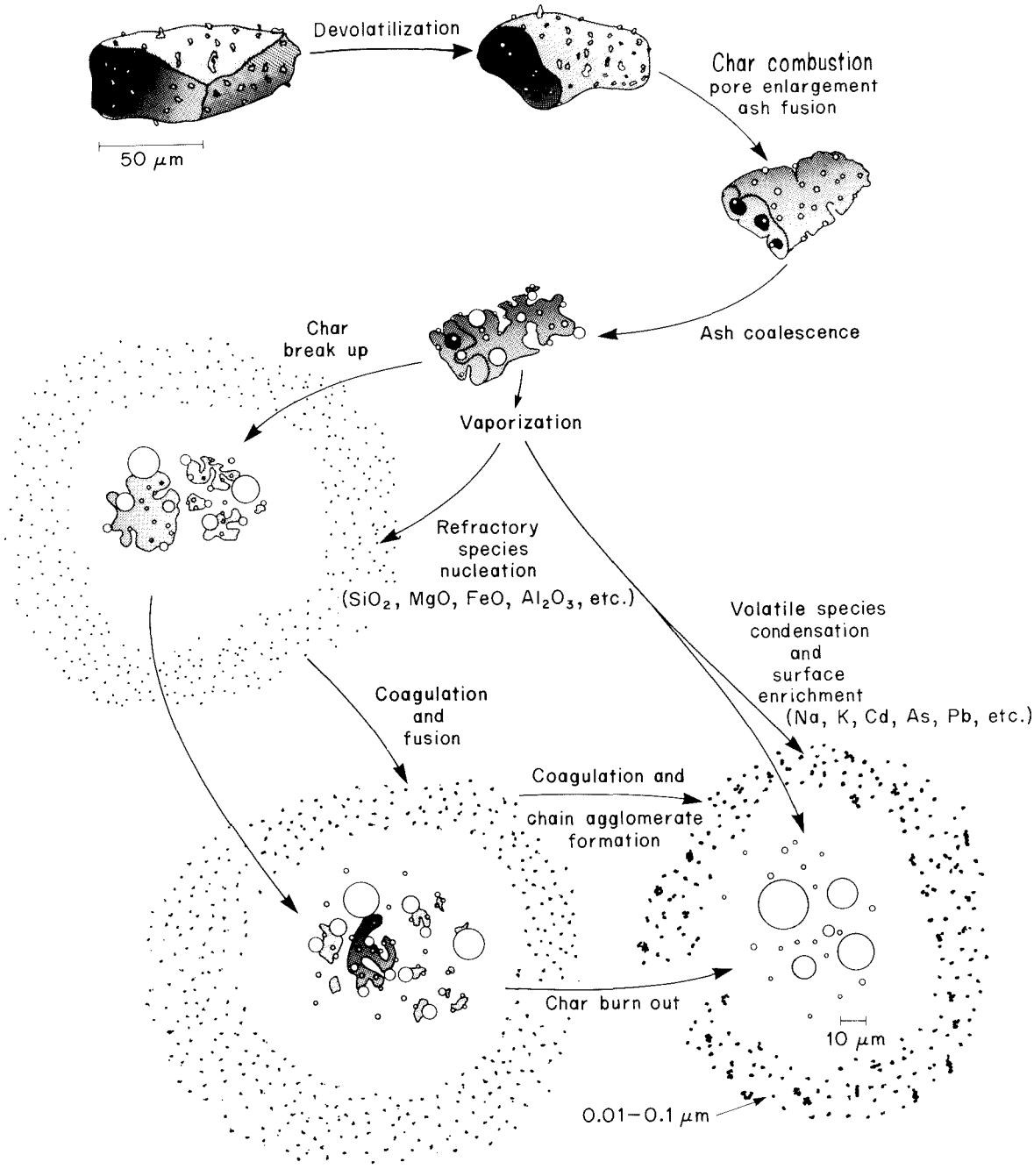

Figure 6.4 Schematic diagram of the processes involved in ash particle formation.

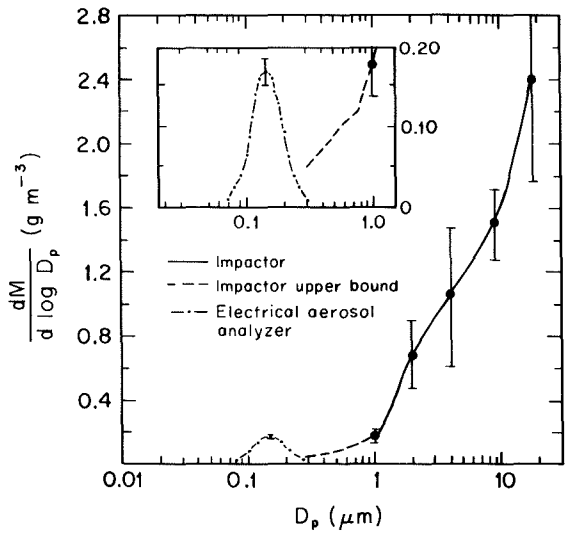

Figure 6.5 Particle size distribution measured upstream of the electrostatic precipitator on a coal-fired utility boiler. Reprinted with permission from Markowski et al., *Environmental Science and Technology*, Vol. 14, No. 11, pp. 1400–1402. Copyright (1980) American Chemical Society.

ticles that have higher densities than the carbonaceous matrix of coal are ground to smaller sizes than are mineral-deficient particles, as indicated clearly in Figure 6.6. The assumption that each coal particle breaks into an equal number of fragments is also an oversimplification. A distribution of fragments will be produced from each coal particle as it burns out. Unfortunately, the nature of that distribution is not well understood at the present time. Nonetheless, the simplistic model in which it is assumed that between 4 and 10 equal-mass ash particles are produced from each coal particle reproduces reasonbly well the general form of observed mass distributions (Flagan and Friedlander, 1978). The distribution of smaller residual ash particles has not yet been resolved, but there are clearly many more small ash particles generated as combustion residues than this simple model would suggest. To explain the sharp peak in the submicron size distribution shown in Figure 6.5, it is necessary to examine the formation of particles from the volatilized ash. We begin with a discussion of the vaporization process.

6.1.3 Ash Vaporization

To understand the vaporization of ash during coal combustion, we must examine the thermodynamics and chemistry of the ash and the transport of the volatilized ash from the surface of the particle. Some components of the ash are highly volatile; examples include sodium, potassium, and arsenic. Volatile ash constituents may vaporize completely during combustion unless inhibited by diffusional resistances, either in transport through the porous structure of the char or to the surfaces of the mineral inclusions. The vaporization process can be a direct transformation from the condensed phase to the vapor phase, for example, for silica,

$$SiO_{2(l)} \rightleftharpoons SiO_{2(v)}$$

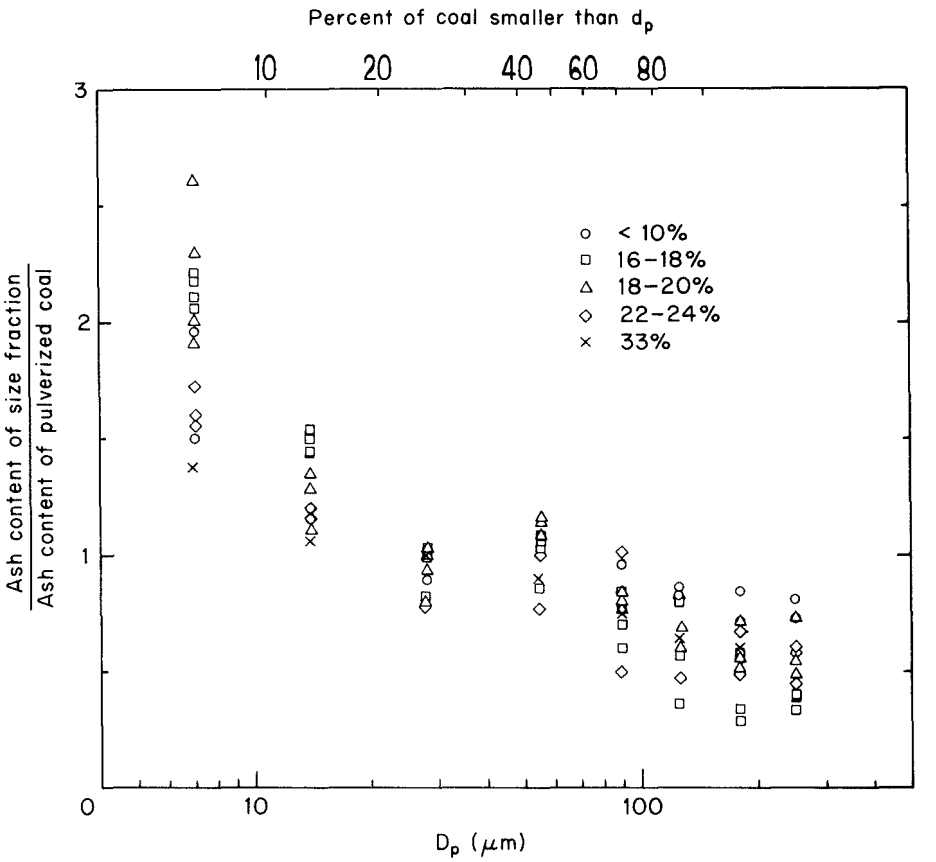

Figure 6.6 Variation of the ash content of pulverized coal with coal particle size (data from Littlejohn, 1966).

or it may involve the production of volatile suboxides or elemental forms from the original oxides,

$$SiO_{2(l)} + CO \rightleftharpoons SiO_{(v)} + CO_2$$

The former mechanism may dominate for the more volatile ash constituents, but there is evidence that the reduction reactions play an important role in the vaporization of species with relatively low vapor pressures.

Predicting the rates of ash vaporization either by direct vaporization or by chemical reaction is difficult. The high-ionic-strength solutions produced as ash melts cannot be described by ideal solution theory, and the vapor pressures above these solutions generally are unknown. Furthermore, resistance to ash vapor diffusion in the porous char is difficult to characterize (Quann and Sarofim, 1982). For vaporization occurring as a result of chemical reactions, the rates and mechanisms of the reactions are needed. Un-

fortunately, little is known about such reactions. Nevertheless, a simple ash vaporization model that assumes vapor equilibrium at the char surface can provide important insights into the factors that govern ash vaporization.

The approach used to predict the ash vaporization rate from a burning char particle is similar to that for evaporation of a droplet. Let us assume that the evaporation of the ash is slow enough that it does not significantly influence either the rate of combustion or the temperature of the char particle. The rate of char combustion, $\bar{r}_c$, and the particle temperature, T_p, can therefore be calculated as outlined in Chapter 2 without reference to the vaporization of the ash. The net mass flux from the particle is equal to the combustion rate (i.e., $\bar{f}_c = \bar{r}_c$). The vapor flux of ash species i from the particle surface may be written as

$$\bar{f}_{is} = \bar{f}_c y_{is} - \rho D \left(\frac{dy_i}{dr}\right)_{r=a} \tag{6.1}$$

where y_i is the mass fraction of species i in the vapor surrounding the particle. The net flux of i from the particle is seen to consist of two contributions: the flux of i carried from the particle surface due to the fluid motion induced by combustion and that due to molecular diffusion in the background gas.

The mass fraction of species i in the vapor is governed by the steady-state continuity equation,

$$4\pi a^2 \bar{f}_c \frac{dy_i}{dr} = \frac{d}{dr}\left(4\pi r^2 \rho D_i \frac{dy_i}{dr}\right) \tag{6.2}$$

subject to the boundary conditions,

$$y_i = y_{is} \qquad r = a$$

$$y_i = y_{i\infty} \qquad r \to \infty$$

Integrating twice, imposing the boundary conditions, and using (6.1) gives

$$\frac{a\bar{f}_c}{\rho D_i} = \ln(1 + B_i) \tag{6.3}$$

where

$$B_i = \frac{y_{is} - y_{i\infty}}{(\bar{f}_i/\bar{f}_c) - y_{is}} \tag{6.4}$$

If we assume that the diffusivity of the vapor species i is equal to that for the combustion gases, $D_i = D$, and from (2.136) and (6.3) we see that $B_i = B_T = B$, the transfer number for combustion. In that case we find

$$\frac{\bar{f}_i}{\bar{f}_c} = \frac{y_{is}(1 + B) - y_{i\infty}}{B} \tag{6.5}$$

If $y_{is} >> y_{i\infty}$, (6.5) further simplifies to

$$\frac{\bar{f}_i}{\bar{f}_c} = y_{is}\left(1 + \frac{1}{B}\right) \tag{6.6}$$

The mass vaporization flux of species i is then

$$\bar{f}_i = \frac{\rho D y_{is}}{a}\left(1 + \frac{1}{B}\right)\ln(1 + B) \tag{6.7}$$

The mass of an ash component that vaporizes as the particle burns is obtained by integrating (6.7) over the particle surface and burning time τ_B, that is,

$$m_i = \int_0^{\tau_B} 4\pi a(t)\rho D y_{is}\left(1 + \frac{1}{B}\right)\ln(1 + B)\,dt \tag{6.8}$$

Assuming that B and y_{is} remain constant throughout the combustion process, (6.8) becomes

$$m_i = y_{is}\left(1 + \frac{1}{B}\right)\int_0^{\tau_B} 4\pi a(t)\rho D \ln(1 + B)\,dt \tag{6.9}$$

The integral in (6.9) is simply the total mass of carbon burned assuming complete combustion. Thus the fraction of the ash species vaporized is

$$\eta_i = \frac{m_i}{m_{i0}} = \frac{y_{is}}{\alpha_i}\left(1 + \frac{1}{B}\right)(1 - \alpha_a) \tag{6.10}$$

where α_i and α_a are the mass fractions of ash species i and total ash, respectively, in the parent coal. For combustion of carbon in air the maximum value of B corresponds to diffusion-limited combustion. Using (2.137) we obtain

$$B_{\max} = \frac{(0.209)(32/28.4)}{16/12} = 0.174$$

so the minimum fraction of ash vaporized is

$$\eta_{i,\min} = 6.75\,\frac{y_{is}}{\alpha_i}(1 - \alpha_a)$$

A reasonable estimate of y_{is} is obtained by assuming that the vapor is at local equilibrium at the particle surface,

$$y_{is} = \frac{p_{ie}M_i}{p\bar{M}} \tag{6.11}$$

where M_i and $\bar{M}$ are the molecular weight of species i and the mean molecular weight of the gas, respectively. Given thermodynamic data on ash and vapor properties, the vaporization rate can thus be estimated. For a minor ash constituent ($\alpha_i << 1$), even low vapor pressure at the surface may lead to complete vaporization.

The actual rate of vaporization of an ash component will be lower than that predicted by the model above because (1) only a fraction of the external surface of the char particle is covered with ash, (2) diffusion of vapor from the inclusions distributed throughout the char volume is restricted by the small pores, and (3) diffusion of volatile species through the ash solution also limits vaporization.

Quann and Sarofim (1982) examined the vaporization of Si, Ca, and Mg during combustion of a number of coals in O_2–N_2 mixtures. In each case, they assumed that vaporization proceeded by reduction of the oxide (MO_n), that is,

$$MO_n + CO \rightleftarrows MO_{n-1} + CO_2$$

Chemical equilibrium was assumed to hold at the surface of the ash,

$$K_p = \frac{p_{Me} p_{CO_2}}{p_{CO}} \tag{6.12}$$

where p_{Me} is the partial pressure of the volatile form of M, and we assume a single-component ash inclusion. If there is no other source of carbon dioxide to influence the local equilibrium, at the surface, (6.12) then gives

$$p_{Me} = p_{CO_2} = (K_p p_{CO})^{1/2} \tag{6.13}$$

The amount of each ash constituent that vaporized during combustion was estimated from measurements of the total quantity of that element in the submicron fume. Using (6.10), the species vapor pressure at the surface of the burning char can then be estimated. The temperature dependence of the vapor pressure of each species was determined using data from a number of controlled laboratory experiments.

Results obtained by Quann and Sarofim (1982) for Ca, Mg, and Si were consistent with the temperature dependence predicted using (6.13), supporting the hypothesis that these ash constituents are volatilized through chemical reduction of the mineral oxides. The net vaporization rate was significantly less than that corresponding to vapor equilibrium at the char surface, suggesting that diffusion resistances within the porous structure of the char retard vaporization, at least for chars in which the mineral matter is dispersed as discrete inclusions (Illinois number 6 and Alabama Rose). The calcium in the Montana lignite is organically bound. As the carbonaceous matter is consumed during burnout, the organically bound calcium must be mobilized. Examination of scanning electron microscope photographs of partially reacted char particles reveals that minute grains are formed on the carbon surface (Quann and Sarofim, 1982). As the burning progresses, the sizes of the ash particles on the char surface continue to increase, ultimately approaching 5 to 10 μm prior to complete combustion. Assuming that the alkaline earths form oxides very early in the combustion process and that those oxides condense as very small inclusions, one predicts that the vaporization rate should approach that predicted for external diffusion control. Figure 6.7 clearly shows that this condition is approached for calcium in the lignite in high-temperature combustion. The decrease in the partial pressure of Ca at lower temperature is thought to result from penetration of oxygen further into the pores of the burning char. The higher oxygen concentration reduces the mole fraction of metal vapors near the surface of the char.

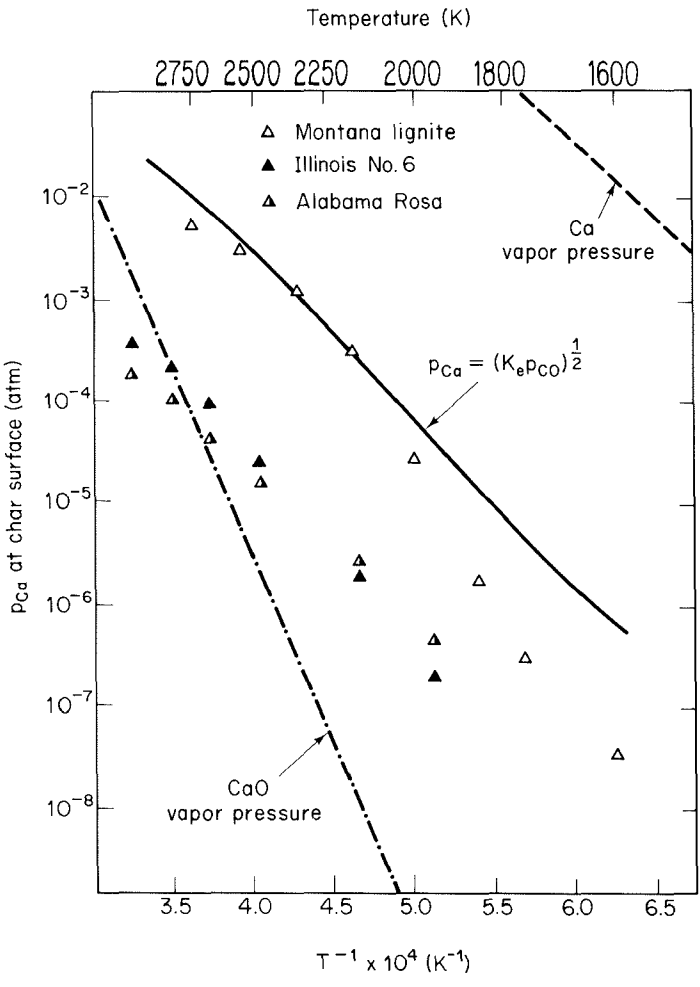

Figure 6.7 Variation of calcium species vapor pressures at the surface of burning coal particles with temperature as inferred from total vaporization measurements. Curves represent equilibrium vapor pressures as noted (Quann and Sarofim, 1982). Reprinted by permission of The Combustion Institute.

Since the enthalpies of volatilization of typical ash constituents are high, the vaporization rates are a strong function of temperature. Fine-particle formation from volatilized ash constituents can be reduced, therefore, by combustion modifications that reduce peak flame temperatures. We recall that control of NO_x formation in coal combustion involves reducing the rate at which air and fuel are brought together. This strategy reduces the peak flame temperature by allowing heat transfer to cool the gases before combustion is complete and, thereby, also reduces fine-particle formation from condensation of volatilized ash components. NO_x and fine-particle formation are thus positively

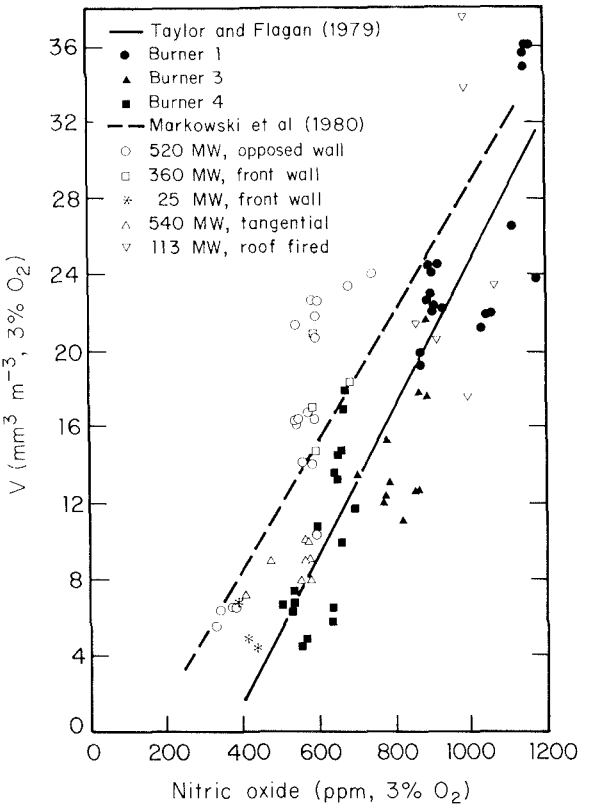

Figure 6.8 Submicron aerosol mass loading measured upstream of control devices in coal-fired utility boilers (open points, dashed line) and in laboratory pulverized coal combustor (solid points, solid line) as a function of NO emissions (Taylor and Flagan, 1981).

correlated (McElroy and Carr, 1981; Taylor and Flagan, 1982) as illustrated by laboratory and field data from a variety of combustors (Figure 6.8).

Extreme measures to control NO_x emissions, however, lead to substantially different impacts on fine-particle formation than those just discussed. The bulk of the ash consists of species that vaporize much more readily in reducing than in oxidizing conditions. Staging the combustion allows a long time in a reducing atmosphere for volatilization of the suboxides to take place, although the lower temperatures may counteract this effect (Linak and Peterson, 1984, 1987). Thus fine-particle formation may actually be favored under such conditions. In laboratory studies of staged combustion, Linak and Peterson (1987) observed an increase of as much as 50% in fine-particle emissions compared with single-stage combustion with the same fuel. As with other aspects of emission control from combustion sources, we again have encountered complex interrelationships between formation and control of different pollutants.

6.1.4 Dynamics of the Submicron Ash Aerosol

During the char burnout phase of coal combustion, much of the heat release occurs at the particle surface, where the carbon is oxidized to carbon monoxide. The hot reducing atmosphere at the surface provides the driving force for ash vaporization. Heat transfer

from the burning particle to the surrounding gases leads to a very sharp temperature gradient in the vicinity of the burning particle. Within a few particle radii, the gas temperature approaches that of the surrounding atmosphere. The oxygen concentration approaches that of the background gas within a similar distance from the particle surface. These sharp gradients dramatically alter the ash vapor equilibrium (Senior and Flagan, 1982).

The resulting supersaturations can be quite high, leading to rapid homogeneous nucleation of some of the ash vapor species within a few radii from the surface of the burning char particle. High supersaturation means that the critical nucleus is very small, on the order of atomic dimensions in some cases. Thus, on a time scale that is comparable to that of char combustion, very large numbers of very small particles can be produced by the nucleation of volatilized ash. Coagulation dominates the growth of these small particles, although condensation can be significant at long times when the temperature is low enough that the volatile ash constituents condense.

When the number concentration is high and coagulation dominates particle growth, the dynamics of the nucleation-generated ash fume can be described by the coagulation equation (5.150). The nucleation-generated ash particles are small enough that the free molecular Brownian coagulation coefficient (5.157) can be applied during most of the growth process. The dynamics of the coagulating kinetic regime ash aerosol can be described approximately using the similarity solution to the coagulation equation that produces the self-preserving particle size distribution function (see Example 5.8).

The self-preserving size distribution model assumes that the only particles present are the small particles. The residual ash particles produced in pulverized coal combustion are sufficiently abundant, however, that the coagulation of the fine, self-preserving mode particles with the large residual ash particles is a significant sink for the former. The loss of fine particles can be estimated if we assume that the loss of fine particles to the coarse particles does not alter the form of the size distribution of the smaller particles and, further, that the accumulation of fine particles does not significantly alter the size distribution of the large particles. We assume further that the size difference between the residual ash particles and the nucleation-generated particles is large. The loss of fine particles to the larger residual ash particles is then a diffusional loss term, allowing us to separate the integrations over the coarse and the fine particles. Assuming the nucleation-generated particles to be in the free molecular size regime, the diffusional flux of the small particles to the surface of the residual ash particles is obtained using the Fuchs-Sutugin interpolation, (5.94).

Predictions of the fine particle size distribution are compared with laboratory measurements of the fine particles produced in pulverized coal combustion in Figure 6.9. For these calculations, the size distribution of the residual ash particles was estimated by assuming that five equal-mass residual ash particles were produced from each parent coal particle. The amount of ash volatilized was matched to the measured fine particle volume for the calculations. The shape of the measured size distribution closely approximates the self-preserving size distribution, and the absolute number concentrations agree quite well.

Attempts to simulate the fine-particle growth in pulverized coal-fired utility boilers

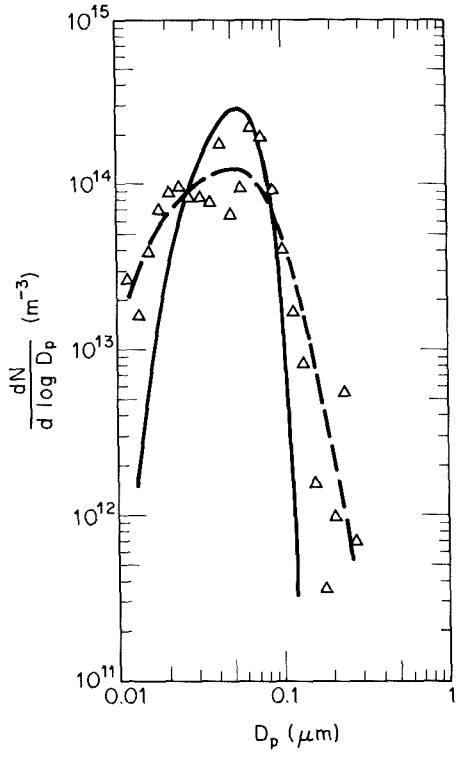

Figure 6.9 Comparison of the submicron ash particle size distribution predicted using the self-preserving aerosol distribution model (solid curve) with size distribution measurements (broken curve) made on a laboratory pulverized coal combustor (Taylor and Flagan, 1981).

(Flagan and Friedlander, 1978; Flagan, 1979) have not been so successful. The number concentrations are generally overestimated by a significant factor. This probably indicates that the residence time during which coagulation proceeds prior to measurement is underestimated, due either to the treatment of the complex flow in the boiler as a plug flow or to coagulation in the sampling system prior to measurement of the size distribution. Nonetheless, these and other studies of fine ash particles produced in pulverized coal combustion clearly demonstrate the role of ash volatilization in fine-particle formation.

6.2 CHAR AND COKE

The carbonaceous char residue that remains after coal is devolatilized burns slowly by surface reactions. If the char particle is too large, mixing in the combustion is poor, or heat is transferred too quickly, char particles may not be fully consumed. Heavy fuel oils may produce similar carbonaceous particles, called *coke*. Coke particles are relatively large, 1 to 50 μm in diameter, with smaller numbers of much larger particles, and account for the majority of particulate mass emitted from boilers fired with heavy fuel oils. They are hard cenospheres, porous carbonaceous shells containing many blowholes

(Marrone et al., 1984). Fuel impurities tend to concentrate in these cenospheres (Braide et al., 1979). Coke particles are formed by liquid-phase pyrolysis of heavy fuel oil droplets. The mechanisms and rates of coke particle formation are not well understood.

In studies of the combustion of individual millimeter-sized droplets of heavy fuel oil, Marrone et al. (1984) identified two combustion times: (1) the droplet burning time, which corresponds to the time required for coke formation, and (2) the time required for the coke particle to burn. During about the first 60% of the droplet burning phase, combustion was relatively quiescent. In the final stages of droplet burning, the droplet deforms and finally appears to froth just prior to forming a small coke cenosphere. Small droplets may be ejected during the latter violent phase of coke formation. Immature coke particles were found to be tarry and soluble in organic solvents. Coke cenospheres that could not be dissolved in organic solvents were produced only at the end of the droplet lifetime. Typically, the coke particles accounted for about 3% of the mass of the residual (heavy component) oil in the original fuel oil droplet, even when the residual oil was diluted with 60% of a light distillate oil. Asphaltine conversion to coke was about 30%.

The influence of fuel droplet size on coke formation is not well documented, but there is evidence that size, at least down to 100 μm, has no effect on the quantitative behavior of burning heavy fuel oil droplets (Marrone et al., 1984). At smaller sizes, droplet lifetimes might be short enough that there would be insufficient time for the coking reactions to go to completion. Observations that the coke formation occurs within 10 to 20 ms suggest that the size of droplet required to prevent coke formation would be small indeed, less than about 20 μm in diameter. Coke particle formation appears to be almost unavoidable in the combustion of heavy fuel oils. Emission rates would be reduced substantially by reducing the time required in coke combustion. Improved atomization or dilution of the heavy fuel oil with a lighter component would decrease the initial size of the coke particles, thereby reducing the combustion time.

6.3 SOOT

Carbonaceous particles can also be produced in the combustion of gaseous fuels and from the volatilized components of liquid or solid fuels. The particles formed by this route, known as *soot*, differ markedly from the char and coke discussed previously. Most commonly, soot particles are agglomerates of small, roughly spherical particles such as those shown in Figure 6.10. While the size and morphology of the clusters can vary widely, the small spheres differ little from one source to another. They vary in size from 0.005 to 0.2 μm but most commonly lie in the size range 0.01 to 0.05 μm (Palmer and Cullis, 1965). The structural similarity between soot particles and the inorganic particles produced from volatilized ash (Figure 6.3) suggests a common origin. The genesis of soot, however, is much less well understood that that of the inorganic particles due to the extreme complexity of hydrocarbon chemistry in the flame, as well as to the fact that soot particles can burn if exposed to oxygen at high temperatures.

The small spheres that agglomerate together to form a soot particle consist of large numbers of lamellar crystallites that typically contain 5 to 10 sheets containing on the

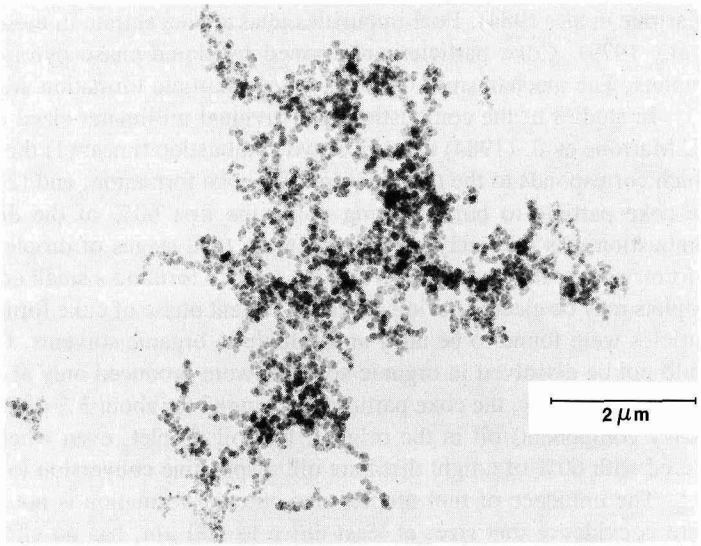

(a)

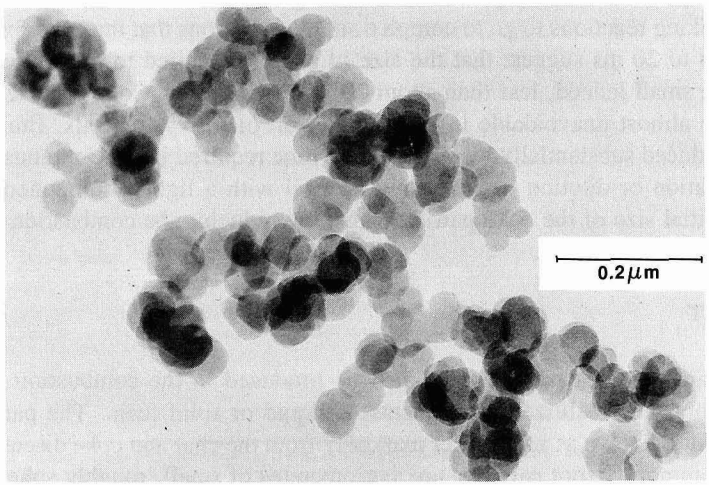

(b)

Figure 6.10 Transmission electron microscope photographs of soot particles produced in a laminar diffusion flame with acetylene fuel illustrating the agglomerate structure (courtesy of E. Steel, National Bureau of Standards).

order of 100 carbon atoms each. The structure within each sheet is similar to that of graphite, but adjacent layers are randomly ordered in a turbostratic structure. The platelets are also randomly oriented and bound by single sheets or amorphous carbon, giving rise to the spherical particles illustrated in Figure 6.11.

Soot particles are not pure carbon. The composition of soot that has been aged in

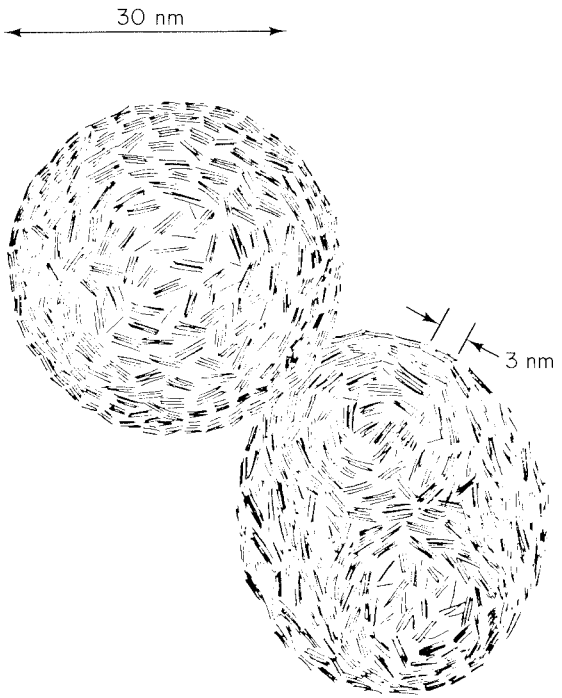

Figure 6.11 Schematic of soot microstructure.

the high-temperature region of the flame is typically C_8H (Palmer and Cullis, 1965), but soot may contain considerably more hydrogen earlier in the flame. Furthermore, soot particles adsorb hydrocarbon vapors when the combustion products cool, frequently accumulating large quantities of polycyclic aromatic hydrocarbons.

The presence of soot in a flame is actually advantageous in certain situations. Because of the high emissivity of soot particles relative to that of the gases in the flame, only a small quantity of soot is sufficient to produce an intense yellow luminosity. Soot is necessary in boiler flames to obtain good radiative heat transfer. The presence of soot is vital to give a candle flame its characteristic yellow appearance. In gas turbines, on the other hand, the intense radiative transfer from soot is to be avoided. Without soot, hydrocarbon flames appear either violet due to emissions from excited CH radicals when fuel-lean or green due to C_2 radical emissions when fuel-rich (Glassman, 1977). In many cases soot serves its purpose as a radiator and is consumed before it leaves the flame. If it does escape the flame, soot poses serious environmental consequences. The high emissivity of soot translates into a high absorptivity at ambient temperatures, leading to its black color in a plume.

6.3.1 Soot Formation

Soot forms in a flame as the result of a chain of events that begins with pyrolysis and oxidative pyrolysis of the fuel into small molecules, followed by chemical reactions that build up larger molecules that eventually get big enough to become very small particles.

The particles continue to grow through chemical reactions at their surface reaching diameters in the range 0.01 to 0.05 μm at which point they begin to coagulate to form chain agglomerates. The C/H ratio of the small particles is about unity, but as soot ages in the flame it loses hydrogen eventually exiting the flame with a C/H ratio of about 8.

Despite numerous studies, our understanding of soot formation, especially the early phases, is incomplete (Glassman, 1979; Smith, 1982; Haynes and Wagner, 1981; Lehaye and Prado, 1981).

Soot formation is favored when the molar ratio of carbon to oxygen approaches 1.0, as suggested by the stoichiometry,

$$C_mH_n + \alpha O_2 \longrightarrow 2\alpha CO + \frac{n}{2} H_2 + (m - 2\alpha) C_s$$

In premixed flames the critical C/O ratio for soot formation is found to be smaller than 1.0, actually about 0.5. The lower C/O ratio suggests that an appreciable amount of the carbon is tied up in stable molecules such as CO_2.

The propensity to form soot (as measured by the critical C/O ratio at which soot formation begins) is a complex function of flame type, temperature, and the nature of the fuel (Glassman and Yaccarino, 1981). There is general agreement that the rank ordering of the sooting tendency of fuel components goes: naphthalenes > benzenes > aliphatics. However, the order of sooting tendencies of the aliphatics (alkanes, alkenes, and alkynes) varies dramatically with flame type. Glassman and Yaccarino (1981) attribute much of the variability to flame temperature. In premixed flames, sooting appears to be determined by a competition between the rate of pyrolysis and growth of soot precursors and the rate of oxidative attack on these precursors (Millikan, 1962). As the temperature increases, the oxidation rate increases faster than the pyrolysis rate, and soot formation decreases.

In diffusion flames, oxygen is not present in the pyrolysis zone, so the increase in the pyrolysis rate with temperature leads to an increasing tendency to soot. Small amounts of oxygen in the pyrolysis zone appear to catalyze the pyrolysis reaction and increase sooting (Glassman and Yaccarino, 1981).

The difference between the sooting tendencies of aromatics and aliphatics is thought to result from different routes of formation. Aliphatics appear to form soot primarily through formation of acetylene and polyacetylenes at a relatively slow rate, illustrated in Figure 6.12. Aromatics might form soot by a similar process, but there is a more direct route involving ring condensation or polymerization reactions that build on the existing aromatic structure (Graham et al., 1975). The fragmentation of aromatics should occur primarily at high temperature, but such reactions may not be important even there (Frenklach et al., 1983). In flames, fuel pyrolysis generally begins at relatively low temperature as the fuel approaches the flame front, so the soot inception process may be completed well before temperatures are high enough to initiate the competitive reactions (Gomez et al., 1984).

Once soot nuclei have been formed, particle growth occurs rapidly by surface reactions (Harris and Weiner, 1983a, b). Ultimately, the soot nuclei account for only a

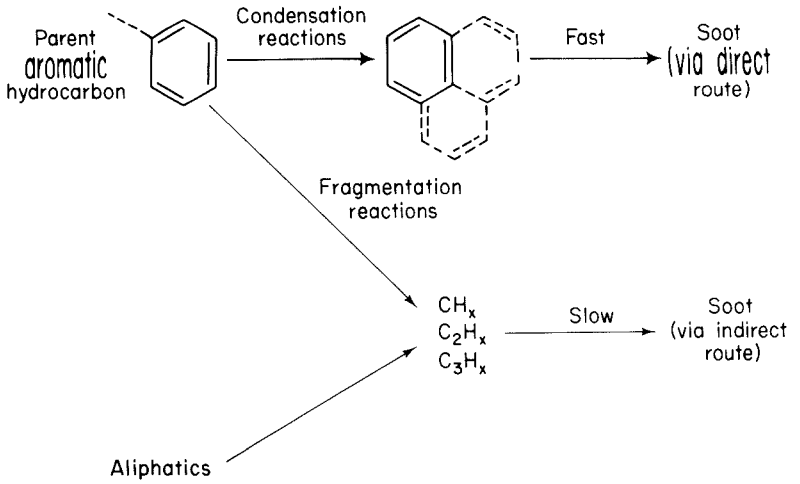

Figure 6.12 Chemical pathways for soot formation.

small fraction of the mass of soot formed; the remainder is material that has condensed or reacted on the initial nuclei. The yield of soot increases rapidly as the C/O ratio increases beyond the sooting threshold (Haynes and Wagner, 1981). Remarkably, while the quantity of soot generated varies dramatically from one flame to another, the surface growth rate of individual particles does not appear to vary significantly with fuel composition or flame characteristics (Harris and Weiner, 1983a, b). The growth rate does vary with the age of the soot, however. Typically, the surface growth rate is 0.4 to 1 g m^{-2} s^{-1} early in the flame, decreases to about 0.1 to 0.2 g m^{-2} s^{-1} after 25 to 30 ms in the flame, and drops precipitously thereafter (Harris and Weiner, 1983a, b). The time scale of this change in growth rate corresponds to that in which the C/H ratio of the soot particles increases from an initial value of about 1 to 8 or so. Therefore, it has been suggested that the changing C/H ratio, in some as yet undefined way, is responsible for the decline in growth rate.

Since the growth rate of soot particles is not a strong function of fuel composition, the wide range of soot emissions is attributed to differences in the number of soot nuclei initially formed. The formation of the soot nuclei is poorly understood. It does not appear to involve homogeneous nucleation, as discussed in Chapter 5. Rather, it appears that a sequence of gas-phase, polymerization reactions produces hydrocarbon molecules of ever-increasing molecular weight until, at a molecular weight on the order of 1000, soot particles are formed (Wang et al., 1983). The soot precursors are large polycyclic aromatic hydrocarbons, so the chemical mechanisms of soot formation are directly related to those discussed in Chapter 3 for the formation of polycyclic aromatic hydrocarbons.

Soot particle inception takes place very early in the flame, in a region where radicals are present in superequilibrium concentrations (Millikan, 1962). In premixed flames, soot inception proceeds for only 2 to 3 ms, during which time the surface growth rate of the nuclei is approximately zero (Harris et al., 1986). In those experiments, the region of soot inception contained about 1% O_2. Similarly, in shock tube studies of soot for-

mation, Frenklach et al. (1985) found that small amounts of oxygen enhance soot formation over that for pyrolysis in an inert atmosphere. Once the oxygen level in the flame declines, new particle inception ceases, and the surface growth rate rises rapidly to a plateau. Oxygen appears to play two major roles: (1) in the oxidative attack of the hydrocarbon molecules, the concentrations of the radicals needed for the polymerization reactions are maintained at high levels; and (2) oxidative attack on the incipient soot nuclei and precursors limits soot growth until the oxygen has been consumed.

In spite of the wealth of experimental data and our improving understanding of the nature and formation of soot, no generally applicable model has yet been formulated to predict soot formation as a function of fuel type and combustion conditions. Harris et al. (1986) have proposed a model for soot particle inception kinetics. Let m_i be the mass of a soot particle containing i units of the smallest soot nuclei. The smallest soot nucleus, of mass m_1, is presumed to be formed directly by reactions of gas-phase species. The rate of change of the number density of particles of size i can then be expressed as

$$\frac{dN_i}{dt} = \left(\frac{dN_i}{dt}\right)_{\text{coagulation}} + \left(\frac{dN_i}{dt}\right)_{\text{inception}} + \left(\frac{dN_i}{dt}\right)_{\text{growth}} + \left(\frac{dN_i}{dt}\right)_{\text{oxidation}} \tag{6.14}$$

The rate of change of N_i by coagulation is represented as outlined in Chapter 5. The inception term is nonzero only for $i = 1$, where $dN_i/dt = I_1(t)$.

In the analysis of Harris et al. (1986), an incipient soot particle was actually defined as the smallest species that absorbs light at a wavelength of 1.09 μm. Such species were argued as likely to be similar to the smallest particles actually observed by Wersborg et al. (1973) that had diameters near 1.5 nm and contained on the order of 100 carbon atoms. The inception rates are thus defined experimentally and theoretically as the flux of particles across this lower limit. The physical mechanism for growth is thought to be the thermal decomposition of acetylene on the surface of existing particles.

Although we will subsequently discuss soot oxidation in more detail, for the purposes of the soot particle dynamics model, Harris et al. (1986) assume that the ratio of surface growth and oxidation are proportional to soot surface area, so the rate of change of the mass of a particle size i from growth and oxidation is

$$\frac{dm_i}{dt} = k(t)s_i \tag{6.15}$$

where s_i is the surface area of a particle of size i, and $k(t)$ is an appropriate rate constant that, according to Harris et al. (1986), varies with time due to the aging of the carbonaceous structure of soot. Thus

$$\left(\frac{dN_i}{dt}\right)_{\text{growth}} + \left(\frac{dN_i}{dt}\right)_{\text{oxidation}} = \frac{|k(t)|}{m_1}\left[N_k s_k - N_i s_i\right] \tag{6.16}$$

where $k = i - 1$ or $i + 1$ depending on whether $k(t)$ is positive (growth rate exceeds oxidation rate) or negative (oxidation rate exceeds growth rate), respectively. When $k(t) < 0$, (6.16) still accounts for surface growth of $i = 1$ particles, but when $k(t) > 0$.

$$\frac{dN_i}{dt} = \frac{-k(t)N_1 s_1}{m_1} \tag{6.17}$$

Growth of a species smaller than size 1 is inception.

In summary, according to the model above, soot particles form by a poorly understood inception process and then grow by coagulation and the impingement of vapor species on their surface. They shrink by oxidation, which is also represented as a surface reaction process, presumably involving the collision of oxidants such as O_2 and OH with the soot particles.

Harris et al. (1986) estimated the soot inception rate in a premixed ethylene–argon–oxygen flame by solving the set of ordinary differential equations for the N_i for diameters between 1.5 nm ($i = 1$) and 22 nm ($i = 3000$), 0.022 μm, to conform with optical data on soot particles obtained in a premixed ethylene flame.* Figure 6.13 shows the soot particle total number density, mean particle diameter, and inception rate, J, as functions of time over positions corresponding to $t = 1.1$ to 9.6 ms beyond the estimated reaction zone of the flame. Figure 6.13 shows the calculated rate of soot particle inception. The data, which start 1.1 ms beyond the reaction zone, missed the rise in the inception rate. Using the curve, the authors estimate that a total of about 10^{19} incipient particles m^{-3} were created in this flame, with a peak new particle formation rate of 10^{23} m^{-3} s^{-1}. This quantity corresponded to 50% of the soot volume present at 2.4 ms, 3% of the soot volume present at 9 ms, and less than 1% of the soot volume ultimately formed.

6.3.2 Soot Oxidation

Soot particles formed in the fuel-rich regions of diffusion flames are eventually mixed with gases sufficiently fuel-lean that oxidation becomes possible. As a result, the soot actually emitted from a combustor may represent only a small fraction of the soot formed in the combustion zone. Since the conditions leading to soot formation in diffusion flames cannot be entirely eliminated, soot oxidation downstream of the flame is very important to the control of soot emissions.

We desire to develop a useful model for soot oxidation. Park and Appleton (1973) observed that the rate of oxidation of carbon black (a commercially produced soot-like material) by oxygen could be described by a semiempirical model originally developed by Nagle and Strickland-Constable (1962) to describe the oxidation of pyrolytic graphite (2.156).

There are other potential oxidants in flames besides O_2. As we have seen, in fuel-rich flames, OH may be more abundant than O_2, and the O and O_2 concentrations may be comparable. Let us estimate the rate of oxidation of a soot particle by reaction with OH. The flux of molecules at a number concentration N impinging on a unit area of surface in a gas is $N\bar{c}/4$, where $\bar{c}$ is the mean molecular speed of the gas molecules, $\bar{c}$

*The authors discuss those physical phenomena that influence the coagulation rate (e.g., van der Waals forces, charging, etc.) together with a variety of assumptions that must be made.

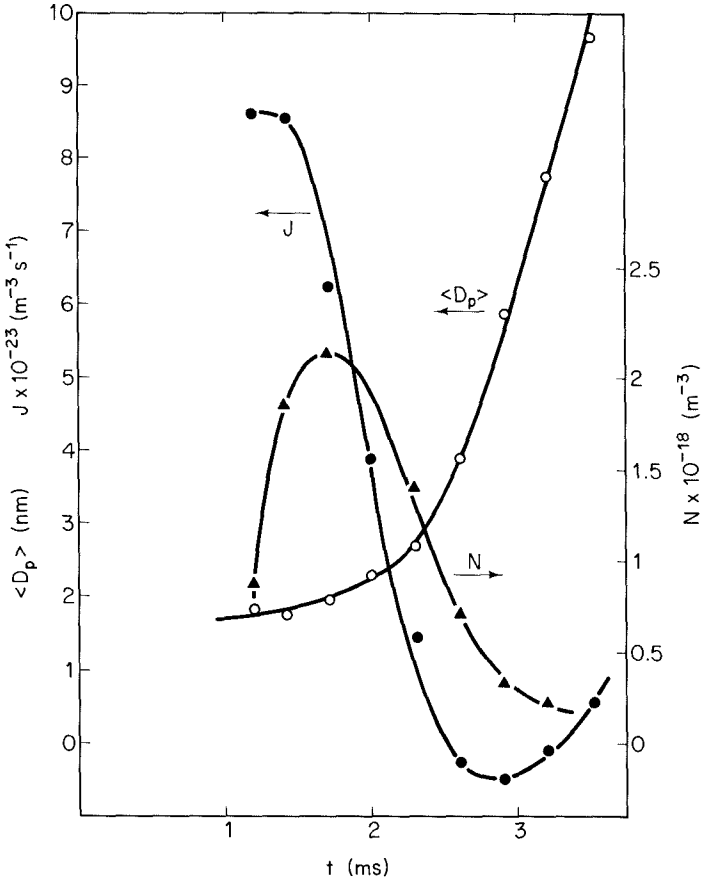

Figure 6.13 Number concentration, mean particle size, and soot particle inception rate as functions of time from the onset of reaction as inferred by Harris et al. (1986) from optical measurements of the soot in a premixed, flat, ethylene-argon-oxygen flame.

$= (8RT/\pi M)^{1/2}$. The rate of oxidation of OH radicals can be estimated as

$$\bar{r}_{OH} = 0.012 k_{OH}[OH] \quad \text{g m}^{-2}\,\text{s}^{-1} \tag{6.18}$$

where $k_{OH} = \gamma_{OH}(RT/2\pi M_{OH})^{1/2}$, where γ_{OH} is the accommodation coefficient for OH on the soot particle surface, the fraction of OH radical collisions with the surface that lead to reaction. Using such a model to analyze soot oxidation by OH, Neoh et al. (1981) found that a value of $\gamma_{OH} = 0.28$ was consistent with their data. With this value of γ_{OH}, $k_{OH} = 2.47T^{1/2}$ g m^{-2} s^{-1} (mol/m^{-3})$^{-1}$.

Rosner and Allendorf (1968) examined the reaction of oxygen atoms with pyrolytic graphite. The accommodation coefficient was found to be weakly dependent on temperature and oxygen partial pressure, varying from about 0.15 to 0.3. Assuming that $\gamma_O =$

0.2, the rate constant for reaction of O with the carbon surface is estimated to be $k_O = 1.82 T^{1/2}$ g m^{-2} s^{-1} (mol m^{-3})$^{-1}$.

The total soot oxidation rate is the sum of the O_2 and OH oxidation rates,

$$\bar{r} = \bar{r}_{O_2} + \bar{r}_{OH} + \bar{r}_O \tag{6.19}$$

Particle burnout is described by

$$\frac{dm_p}{dt} = -\bar{r}A \tag{6.20}$$

where A is the surface area. For spherical particles, the rate of change of the radius is

$$\frac{da}{dt} = \frac{-\bar{r}}{\rho_p} \tag{6.21}$$

Soot particle densities are typically $\rho_p \simeq 1800$ kg m^{-3}.

Figure 6.14 shows the calculated surface recession velocity as a function of equiv-

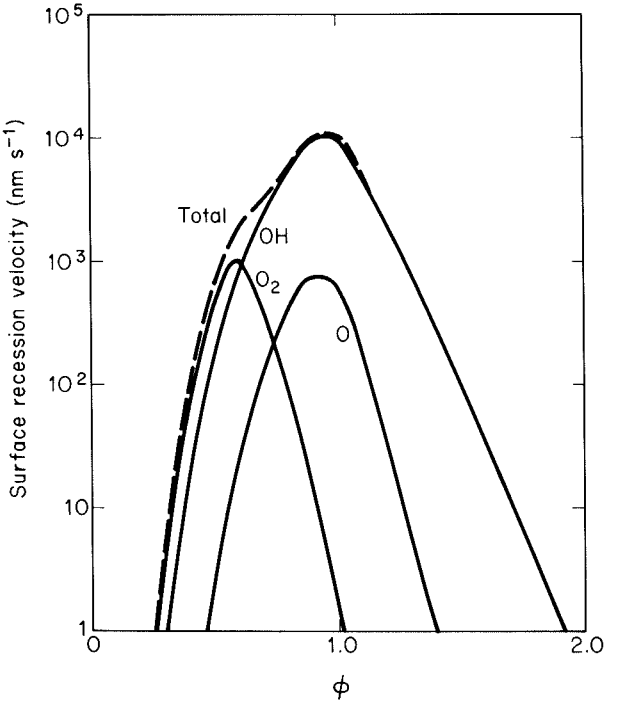

Figure 6.14 Variation of the surface recession rate of soot particles with equivalence ratio for adiabatic combustion of a fuel with composition $CH_{1.8}$.

alence ratio for equilibrium adiabatic combustion. For $\phi < 0.7$, the O_2 reaction dominates, although the OH reaction is still important. As the combustion products are cooled, the equilibrium OH level will drop, reducing the contribution of that reaction. Near stoichiometric and in fuel-rich combustion products, the OH reaction clearly dominates.

The spherical soot particles are typically 10 to 50 nm in diameter. The time to burn the soot particle completely is

$$\tau_B = \frac{\rho_p}{\bar{r}} \frac{D_p}{2}$$

The time to burn a 20-nm-diameter soot particle is about 1 ms at stoichiometric conditions. Thus soot particles burn rapidly when they pass through the flame front. Very rapid dilution with cold air, however, may lead to soot emissions in spite of an abundance of oxygen.

6.3.3 Control of Soot Formation

The range of equivalence ratios over which reactions critical to soot formation and destruction take place is very broad. Turbulent mixing again strongly influences the emission levels from most practical combustors. Soot formation takes place only in the extreme fuel-rich portion of the combustion region, but all fuel must pass through this domain in nonpremixed combustors. Soot oxidation takes place closer to the mean composition. Since, as we have seen, soot oxidation is rapid near stoichiometric conditions, there should be ample opportunity for soot to burn out in a well-mixed combustor.

Prado et al. (1977) have clearly demonstrated these effects using the plug flow combustor described in Chapter 2. An air-blast atomizer was used to inject liquid fuels and, at the same time, to control the turbulent intensity in the first two diameters ($\sim$20 ms residence time) along the length of the combustor. Their results for the stoichiometric combustion of kerosene are shown in Figure 6.15. The soot level rises rapidly in the first diameter along the combustor (100 cm). The rapid increase in the soot loading then abruptly terminates. At high atomizing pressures, the soot loading then drops relatively slowly by an order of magnitude or more, whereas the soot level remains approximately constant at low atomizing pressure.

Previous studies by Pompei and Heywood (1972) using the same combustor under similar conditions showed that most of the oxygen and, therefore, most of the fuel were consumed in the first two diameters of the combustor, with the final consumption of oxygen proceeding much more slowly due to decreasing mixing rates. At the low atomizing pressure ($\Delta p \simeq 82$ kPa) the oxygen level became essentially constant at about the same point where the soot plateau begins (see Figure 6.15), clearly indicating that poor mixing is allowing soot to survive even though there is enough oxygen to consume it fully. Higher mixing rates do not necessarily prevent soot formation; they simply provide the opportunity for soot formed early in the combustor to burn. While increasing

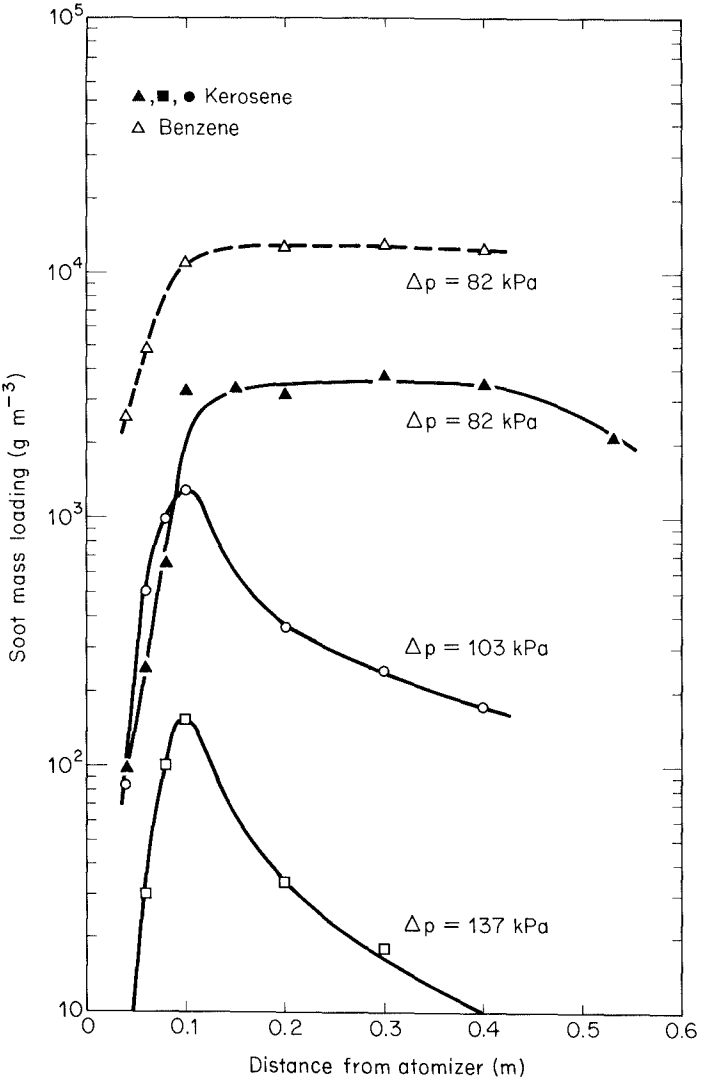

Figure 6.15 Soot mass loadings as a function of axial position in a plug flow combustor. Data for combustion of kerosene using various pressures of an air-assist atomizer are shown as solid points. Measurements for benzene combustion are shown as open points (data from Prado et al., 1977). Reprinted by permission of The Combustion Institute.

the mixing rate in these experiments reduced the peak soot levels by a factor of 20, the exhaust levels were reduced by more than two orders of magnitude.

In the portion of the combustor where soot was being oxidized, the mean size of the basic spherical elements of the soot particles did not decrease, as might be expected if the soot were slowly oxidized, but rather increased. The increased was attributed to the more rapid combustion of the smaller particles. An examination of the soot oxidation rates plotted in Figure 6.14 clearly shows that burnout of the 19- to 25-mm-diameter soot particles should be very rapid once they approach stoichiometric conditions. Thus the question does not appear to be how rapidly the soot will burn but whether it will have the opportunity to burn at all.

Air-blast atomizers introduce a small amount of air directly into the fuel spray and produce the intense mixing necessary to promote soot burnout. Because of their reduced smoke formation, air-blast atomizers have largely displaced pressure atomizers in aircraft gas turbine engines (Mellor, 1981). Pressure atomizers (in which pressurized liquid is sprayed directly through an orifice), nonetheless, are still used in many applications, most notably in diesel engines but also in small stationary furnaces. Improved mixing through atomizer changes may be a suitable option for soot emission control in many cases. The diesel engine, however, has a number of special problems due to its cyclic operation.

Small quantities of various substances, particularly metals, have a profound effect on the sooting behavior of both premixed and diffusion flames. Both pro- and anti-sooting effects can be exhibited by the same additive under different conditions (Haynes et al., 1979). Sodium, potassium, and cesium salts have been observed to increase the soot yield greatly. Barium undergoes chemi-ionization by such reactions as

$$\mathrm{Ba + OH \longrightarrow BaOH^+ + e^-}$$
$$\mathrm{BaO + H \longrightarrow BaOH^+ + e^-}$$

Large ion concentrations (10^{16} to 10^{19} $\mathrm{m^{-3}}$) are produced by the addition of only a few parts per million of these additives in the fuel (Haynes et al., 1979). These ions do not appear to reduce significantly the total amount of soot formed. Pronounced shifts in the mean particle size have been observed from 50 to 16 nm after 30 ms in a premixed flame. This shift was attributed to a reduction in the coagulation rate due to electrostatic repulsion between the charged particles. In an earlier work, Bulewicz et al. (1975) observed enhanced soot formation for small additions of these species, but soot inhibition at higher additive concentrations in a diffusion flame. The smaller soot particles burn faster than the larger ones produced without the additives, leading to lower soot emissions from the diffusion flame (Howard and Kausch, 1980).

Alkaline earths (Ca, Sr, Ba) form their hydroxides from the sequence (Glassman, 1977)

$$\mathrm{M + H_2O \longrightarrow MOH + H}$$
$$\mathrm{MOH + H_2O \longrightarrow M(OH)_2 + H}$$

in which M represents the alkaline earth metal. H atoms may attack water to form OH, that is,

$$H + H_2O \longrightarrow OH + H_2$$

In oxygen-deficient fuel-rich flames, this additional production of OH can dramatically increase the oxidation of soot precursors and prevent soot formation.

Transition metal additives, notably Co, Fe, Mn, and Ni, can reduce the quantity of soot emitted without significantly altering the particle size distribution. Two of the best known commercial additives, methylcylopentadienyl manganese tricarbonyl (MMT) and ferrocene (dicyclopentadrenyl iron), act by this mechanism (Howard and Kausch, 1980). These additives have no effect on the amount of soot formed in a premixed fuel-rich flame, but may increase the rate of oxidation by as much as 20%. Metal oxides may be incorporated in the soot particles and then catalyze soot oxidation by a reaction such as

$$M_xO_y + C_{(s)} \longrightarrow CO + M_xO_{y-1}$$

The emissions of the metal additives can become significant. Giovanni et al. (1972) reported an increase in particulate emissions from turbojet engines by 0.5 g (kg of fuel)$^{-1}$ above the baseline emissions of 2 to 14 g (kg of fuel)$^{-1}$ when manganese was used to reduce soot emissions. The increased emissions were attributed solely to the emissions of manganese in the aerosol.

6.4 MOTOR VEHICLE EXHAUST AEROSOLS

Figure 6.16 shows the volume distribution of primary automobile exhaust aerosols produced under cruise conditions with leaded fuel from a single vehicle as reported by Miller et al. (1976). At speeds up to 35 mph the mode in the volume distribution is at about 0.04 μm, whereas at 50 mph the mode is shifted to about 0.1 μm. Figure 6.17

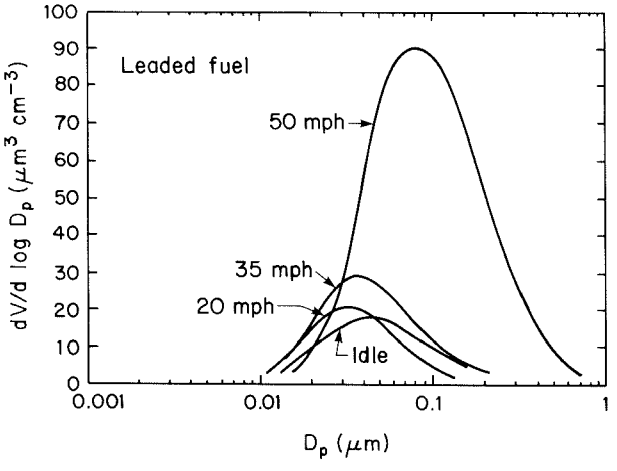

Figure 6.16 Volume distributions of primary automobile exhaust aerosol produced under cruise conditions during combustion of leaded gasoline as reported by Miller et al. (1976). (Reprinted by permission of Air Pollution Control Association).

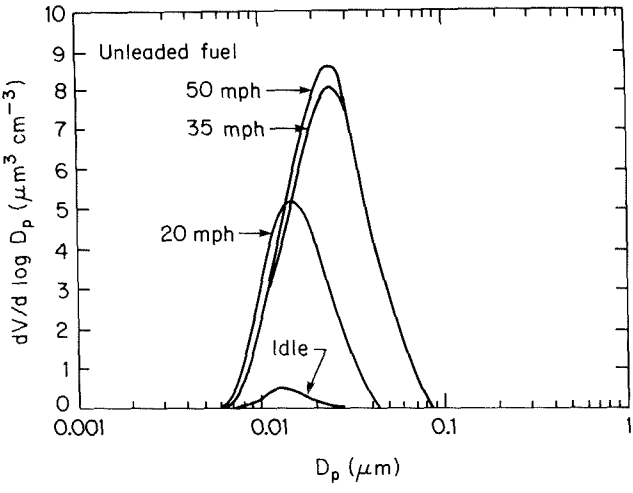

Figure 6.17 Volume distributions of primary automobile exhaust aerosol produced under cruise conditions during combustion of unleaded gasoline as reported by Miller et al. (1976). (Reprinted by permission of Air Pollution Control Association).

shows the aerosol volume distributions from an identical vehicle equipped to run on unleaded fuel. Unlike the case with leaded fuel, the mode in the volume distribution remains between 0.01 and 0.03 μm for all cruise speeds investigated. The shift to slightly larger mean sizes between 20 and 35 mph was attributed to increase gas-to-particle conversion. We note that the conditions leading to the increase in aerosol volume at high speeds with leaded fuel appear to be absent in the case of unleaded fuel combustion. Because the data shown in Figures 6.16 and 6.17 represent a very limited sample, they should not be viewed as indicative of all motor vehicle exhaust aerosols. Nevertheless, they do exhibit the general features with respect to size distribution of automobile exhaust aerosols.

Pierson and Brachaczek (1983) reported the composition and emission rates of airborne particulate matter from on-road vehicles in the Tuscarora Mountain Tunnel of the Pennsylvania Turnpike in 1977. Particulate loading in the tunnel was found to be dominated by diesel vehicles, even though on the average they constituted only about 10% of the traffic. Diesel emission rates were of the order 0.87 g km^{-1}, the most abundant component of which is carbon, elemental and organic. Thirty-four elements were measured, in descending order of mass, C, Pb, H, SO_4^{2-}, and Br together accounting for over 90%. Size distributions of motor vehicle particulate matter exhibited a mass median diameter of 0.15 μm.

Diesel particulate matter consists primarily of combustion-generated carbonaceous soot with which some unburned hydrocarbons have become associated (Amann and Siegla, 1982). Photomicrographs of particles collected from the exhaust of a passenger car diesel indicate that the particles consist of cluster and chain agglomerates of single spherical particles, similar to the other soot particles and the fly ash fume described previously. The single spherical particles vary in diameter between 0.01 and 0.08 μm, with the most usually lying in the range 0.015 to 0.03 μm. Volume mean diameters of the particles (aggregates) tend to range from 0.05 to 0.25 μm. The diesel particulate matter is normally dominated by carbonaceous soot generated during combustion. In addition, 10 to 30% of the particulate mass is comprised of solvent-extractable hydro-

carbons that adsorb or condense on the surface of the soot particles and that consist of high-boiling-point fractions and lubricating oil.

PROBLEMS

6.1. The amount of ash vaporized during coal combustion is typically about 1% of the mineral matter in the coal. Reduced vapor species are oxidized as they diffuse from the surface of the burning char particle leading to rapid homogeneous nucleation and the formation of large numbers of very small particles. Assuming that the initial nuclei are 0.001 μm in diameter and the ash density is 2300 kg m^{-3}, compute and plot the particle number concentration as a function of residence time in the furnace, assuming the gas temperature is 1700 K for 1 second and then decreases to 400 K at a rate of 500 K s^{-1}. The gas viscosity may be taken as $\mu = 3.4 \times 10^{-7} T^{0.7}$ kg m^{-1} s^{-1}. The aerosol may be assumed to be monodisperse.

6.2. A 50-μm-diameter char particle is burned in air in a furnace that is heated to 1800 K. Examine the volatilization of silica (SiO_2) from this particle as it burns. Silica may vaporize directly

$$SiO_{2(c)} \overset{1}{\rightleftharpoons} SiO_{2(v)} \qquad K_{p1} = 2.4 \times 10^8 e^{-69{,}000/T} \text{ atm}$$

or by means of reduction to the monoxide

$$SiO_{2(c)} + CO \overset{2}{\rightleftharpoons} SiO_{(v)} + CO_2 \qquad K_{p2} = 4.53 \times 10^8 e^{-61{,}672/T} \text{ atm}$$

The oxidation rate expression of the char is that for the Whitwick coal in Table 2.10.

(a) Calculate the equilibrium partial pressures for SiO_2 and SiO at the surface of the char particle.

(b) What vaporization rate corresponds to this partial pressure?

(c) Compare the vaporization rate with that predicted for a pure silica particle of the same size. Assume the silica particle temperature is the same as that of the gas.

6.3. For the conditions of Problem 6.2, compute the vapor concentration profile as a function of distance from the surface of the particle, assuming that no condensation takes place. The binary diffusivity may be calculated from $cD = 9.1 \times 10^7 \overline{T} + 7.4 \times 10^{-4}$ mole m^{-1} s^{-1}, where $\overline{T}$ is the mean of gas and particle temperatures. Neglecting vapor loss, calculate and plot the supersaturation ratio and homogeneous nucleation rate. How far from the surface will nucleation occur?

Use the following properties:

Surface tension:	$\sigma = 0.30$ J m^{-2}
Density:	$\rho_c = 2200$ kg m^{-3}
Molecular Weight:	$M = 60.9$ g mole^{-1}

6.4. Harris et al. (1986) observed that no growth of the soot nuclei occurred in the region of the flame where particles are formed and that the oxygen mole fraction in this region is about 0.01. Assuming that the Nagle and Strickland-Constable kinetics describe the oxidation of the soot nuclei and that the growth species is acetylene, estimate the minimum acetylene concentration that would be required to maintain the observed soot nucleus size of 1.8 nm, for temperatures ranging from 1200 K to 1500 K. The flux of acetylene reaching the particle surface may be taken as the effusion flux, and the reaction probability is unity for this estimate. The soot particle density is 1800 kg m^{-3}

REFERENCES

AMANN, C. A., and SIEGLA, D.C., "Diesel Particulates—What They Are and Why," *Aerosol Sci. Technol. 1*, 73–101 (1982).

BRAIDE, K. M., ISLES, G. L., JORDAN, J. B., and WILLIAMS, A. "The Combustion of Single Droplets of Some Fuel Oils and Alternative Liquid Fuel Combinations," *J. Inst. Energy, 52*, 115–124 (1979).

BULEWICZ, E. M., EVANS, D. G., and PADLEY, P. J. "Effect of Metallic Additives on Soot Formation Processes in Flames," in *Fifteenth Symposium (International) on Combustion*, The Combustion Institute, Pittsburgh, PA, 1461–1470 (1975).

DAVISON, R. L., NATUSCH, D. F. S, WALLACE, J. R., and EVANS, C. A., JR. "Trace Elements in Fly Ash—Dependence of Concentration on Particle Size," *Environ. Sci. Tecvhnol., 8*, 1107–1113 (1974).

FLAGAN, R. C. "Submicron Aerosols from Pulverized Coal Combustion," *Seventeenth Symposium (International) on Combustion*, The Combustion Institute, Pittsburgh, PA, 97–104 (1979).

FLAGAN, R. C., and FRIEDLANDER, S. K., "Particle Formation in Pulverized Coal Combustion: A Review," in *Recent Developments in Aerosol Science*, D. T. Shaw, Ed., Wiley, New York, 25–59 (1978).

FRENKLACH, M., RAMACHANDRA, M. K., and MATULA, R. A. "Soot Formation in Shock Tube Oxidation of Hydrocarbons," in *Twentieth Symposium (International) on Combustion*, The Combustion Institute, Pittsburgh, PA, 871–878, (1985).

FRENKLACH, M., TAKI, S., and MATULA, R. A. "A Conceptual Model for Soot Formation in Pyrolysis of Aromatic Hydocarbons," *Combust. Flame, 49*, 275–282 (1983).

GIOVANNI, D. V., PAGNI, P. J., SAWYER, R. F., and HUGHES, L. "Manganese Additive Effects on the Emissions from a Model Gas Turbine Combustor," *Combust. Sci. Tech., 6*, 107–114 (1972).

GLASSMAN, I. *Combustion*, Academic Press, New York (1977).

GLASSMAN, I. "Phenomenological Models of Soot Processes in Combustion Systems," Princeton University Department of Mechanical and Aerospace Engineering Report No. 1450 (1979).

GLASSMAN, I., and YACCARINO, P. "The Temperature Effect in Sooting Diffusion Flames," in *Eighteenth Symposium (International) on Combustion*, The Combustion Institute, Pittsburgh, PA, 1175–1183, (1981).

GOMEZ, A., SIDEBOTHAM, G., and GLASSMAN, I. "Sooting Behavior in Temperature-Controlled Laminar Diffusion Flames," *Combust. Flame, 58*, 45–57 (1984).

GRAHAM, S. C., HOMER, J. B., and ROSENFELD, J. L. J. "The Formation and Coagulation of Soot Aerosols Generated in Pyrolysis of Aromatic Hydrocarbons," *Proc. R. Soc. London-A344*, 259–285 (1975).

HARRIS, S. J., and WEINER, A. M. "Surface Growth of Soot Particles in Premixed Ethylene/Air Flames," *Combust. Sci. Technol., 31*, 155–167 (1983a).

HARRIS, S. J., and WEINER, A. M. "Determination of the Rate Constant for Soot Surface Growth," *Combust. Sci. Technol., 32*, 267–275 (1983b).

HARRIS, S. J., WEINER, A. M., and ASHCRAFT, C. C. "Soot Particle Inception Kinetics in a Premixed Ethylene Flame," *Combust. Flame, 64*, 65–81 (1986).

HAYNES, B. S., and WAGNER, H. G. "Soot Formation," *Prog. Energy Combust. Sci., 7*, 229–273 (1981).

HAYNES, B. S., JANDER, H., and WAGNER, H. G. "The Effect of Metal Additives on the For-

mation of Soot in Combustion," in *Seventeenth Symposium (International) on Combustion*, The Combustion Institute, Pittsburgh, PA, 1365–1374, (1979).

HOWARD, J. B., and KAUSCH, W. J., JR. "Soot Control by Fuel Additives," *Prog. Energy Combust. Sci. 6*, 263–276 (1980).

LEHAYE, J., and PRADO, G. "Morphology and Internal Structure of Soot and Carbon Blacks," in *Particulate Carbon: Formation during Combustion*, D. C. Siegla and G. W. Smith, Eds., Plenum Press, New York, 33–56, (1981).

LINAK, W. P., and PETERSON, T. W. "Effect of Coal Type and Residence Time on the Submicron Aerosol Distribution from Pulverized Coal Combustion," *Aerosol Sci. Technol., 3*, 77–96 (1984).

LINAK, W. P., and PETERSON, T. W. "Mechanisms Governing the Composition and Size Distribution of Ash Aerosols in a Laboratory Pulverized Coal Combustor," in *Twenty-first Symposium (International) on Combustion*, The Combustion Institute, Pittsburgh, PA, (1987).

LITTLEJOHN, R. F. "Mineral Matter and Ash Distribution in 'As-Fired' Samples of Pulverized Fuel," *J. Inst. Fuel, 39*, 59–67 (1966).

MARKOWSKI, G. R., ENSOR, D. S., HOOPER, R. G., and CARR, R. C., "A Submicron Aerosol Mode in Flue Gas from a Pulverized Coal Utility Boiler," *Environ. Sci. Technol., 14*, 1400–1402 (1980).

MARRONE, N. J., KENNEDY, I. M., and DRYER, F. L. "Coke Formation in the Combustion of Isolated Heavy Oil Droplets," *Combust. Sci. Tech., 36*, 149–170 (1984).

MCELROY, M. W., and CARR, R. C. in "Proceedings of Joint Symposium on Stationary Combustion NO_x Control," Electric Power Research Institute Report No. WS-79-220, Palo Alto, CA, 183–199 (1981).

MELLOR, A. M. "Soot Studies in Gas Turbine Combustors and Other Turbulent Spray Flames," in *Particulate Carbon: Formation during Combustion*, D. C. Siegla, Ed., Plenum Press, New York, 343–349 (1981).

MILLER, D. F., LEVY, A., PUI, D. Y. H., WHITBY, K. T., and WILSON, W. E., JR. "Combustion and Photochemical Aerosols Attributable to Automobiles," *J. Air Pollut. Control Assoc., 26*, 576–581 (1976).

MILLIKAN, R. C. "Nonequilibrium Soot Formation in Premixed Flames," *J. Phys. Chem., 66*, 794–799 (1962).

NAGLE, J., and STRICKLAND-CONSTABLE, R. F. "Oxidation of Carbon between 1000–2000°C," in *Proceedings of the Fifth Carbon Conference, 1*, 154–164 (1962).

NEOH, K. G., HOWARD, J. B., and SAROFIM, A. F. "Soot Oxidation in Flames," in *Particulate Carbon: Formation during Combustion*, D. C. Siegla and G. W. Smith, Eds., Plenum Press, New York, 261–282 (1981).

PALMER, H. B., and CULLIS, C. F. "The Formation of Carbon from Gases," in *Chemistry and Physics of Carbon*, P. L. Walker, Ed., Vol. 1, Marcel Dekker, New York, 265–325 (1965).

PARK, C., and APPLETON, J. P. "Shock Tube Measurements of Soot Oxidation Rates," *Combust. Flame, 20*, 369–379 (1973).

PIERSON, W. R., and BRACHACZEK, W. W. "Particulate Matter Associated with Vehicles on the Road: II," *Aerosol Sci. Technol., 2*, 1–40 (1983).

POMPEI, F., and HEYWOOD, J. B. "The Role of Mixing in Burner Generated Carbon Monoxide and Nitric Oxide," *Combust. Flame, 19*, 407–418 (1972).

PRADO, G. P., LEE, M. L., HITES, R. A., HOULT, D. P., and HOWARD, J. B. "Soot and Hydrocarbon Formation in a Turbulent Diffusion Flame," in *Sixteenth Symposium (International) on Combustion*, The Combustion Institute, Pittsburgh, PA, 649–661, (1977).

QUANN, R. J., and SAROFIM, A. F. "Vaporization of Refractory Oxides during Pulverized Coal

Combustion," in *Nineteenth Symposium (International) on Combustion,* The Combustion Institute, Pittsburgh, PA, 1429–1440, (1982).

ROSNER, D. E., and ALLENDORF, H. D. "Comparative Studies of the Attack of Pyrolytic and Isotropic Graphite by Atomic and Molecular Oxygen at High Temperatures," *AIAA J., 6,* 650–654 (1968).

SAROFIM, A. F., HOWARD, J. B., and PADIA, A. S. "The Physical Transformation of the Mineral Matter in Pulverized Coal under Simulated Combustion Conditions," *Combust. Sci. Tech. 16,* 187–204 (1977).

SENIOR, C. L., and FLAGAN, R. C. "Ash Vaporization and Condensation during the Combustion of a Suspended Coal Particle," *Aerosol Sci. Tech., 1,* 371–383 (1982).

SMITH, G. W. "A Simple Nucleation/Depletion Model for the Spherule Size of Particulate Carbon," *Combust. Flame, 48,* 265–272 (1982).

TAYLOR, D. D., and FLAGAN, R. C. "Laboratory Studies of Submicron Particles from Coal Combustion," *Eighteenth Symposium (International) on Combustion,* The Combustion Institute, Pittsburgh, PA, 1227–1237 (1981).

TAYLOR, D. D., and FLAGAN, R. C. "The Influence of Combustor Operating Conditions on Fine Particles from Coal Combustion," *Aerosol Sci. Tech., 1,* 103–117 (1982).

WANG, T. S., MATULA, R. A., and FARMER, R. C. "Combustion Kinetics of Soot Formation from Toluene," in *Nineteenth Symposium (International) on Combustion,* The Combustion Institute, Pittsburgh, PA, 1149–1158 (1983).

WERSBORG, B. L., HOWARD, J. B., and WILLAMS, G. C. "Physical Mechanisms in Carbon Formation in Flames," in *Fourteenth Symposium (International) on Combustion,* The Combustion Institute, Pittsburgh, PA, 929–940 (1973).